Development and Verification of a Computational Model of the Knee Joint for the Evaluation of Surgical Treatments for Osteoarthritis

R. Mootanah[§†]*, C. Imhauser[∫], F. Reisse[§], D. Carpanen[§], R.W. Walker[§], M. Koff[∫∫], M. Lenhoff[∫∫∫], R. Rozbruch[∫∫∫∫], A. Fragomen[∫∫∫∫], Y. Kirane[∫∫∫], K. Cheah[†§], J.K. Dowell[§], H.J. Hillstrom[∫∫∫§]

§ Medical Engineering Research Group, Department of Computing and Technology, Anglia Ruskin University, Chelmsford, Essex, UK

∫Department of Biomechanics, Hospital for Special Surgery, New York, USA

∫∫Department of Radiology and Imaging, Hospital for Special Surgery, New York, USA

∫∫∫ Leon Root Motion Analysis Laboratory, Department of Rehabilitation, Hospital for Special Surgery, New York, USA

∫∫∫∫ Limb Lengthening and Complex Reconstruction Services, Hospital for Special Surgery, New York, USA

† Department of Orthopaedic, Capio Springfield Hospital, Chelmsford, Essex, UK

√Department of Orthopaedic, Mid-Essex Hospital Services Trust, Broomfield Hospital, Essex, UK

*Correspondence details: Rajshree Mootanah, rajshree.mootanah@anglia.ac.uk

Keywords: subject-specific verification a knee finite element model, knee osteoarthritis, medical imaging techniques, finite element model of the knee joint, contact mechanics in the tibio-femoral joint.

Development and Verification of a Computational Model of the Knee Joint for the Evaluation of Surgical Treatments for Osteoarthritis

Introduction: Osteoarthritis (OA) is a debilitating degenerative disease which causes significant pain and loss of joint function, accounts for 1% of total deaths worldwide and costs 1% of UK's gross national product. Excessive joint stress is one major primary biomechanical contributing factor to OA onset and progression. Information about peak joint contact stresses could help plan conservative surgical procedures to relieve damaged tissues from excessive loading, delaying the onset and progression of OA and the need for a total knee arthroplasty. However, stress cannot be measured in vivo and the use of computational methods can yield useful information about joint mechanics.

Aim: Therefore, the aim of this study is to develop and verify a three-dimensional (3D) computational model of a knee joint that integrates pre-operative imaging, motion analysis and computational biomechanics to predict post-operative knee joint mechanics (joint stress magnitude and location). Our ultimate goal is to use this validated FE model to predict the relative effectiveness of different surgical treatments for knee OA.

Methods: High resolution medical imaging (MRI) scans of a cadaveric knee were acquired, using an eight-channel transit-receive phased array coil and SPGR and XETA sequences to generate volumetric datasets for the segmentation and accurate visualisation of the joint tissues. These datasets were employed to create accurate 3D geometries of bone, cartilage, meniscus, and ligament strucures, using Mimics V14.2 imaging package. The 3D models were then exported to computer aided design package CATIA V15R18 and finite element (FE) software ABAQUS V6.11-2, where a model of the knee was created, material properties and boundary conditions emulating upright position and gait were applied, and sensitivity analyses on element size and material properties were performed. The cadaveric knee was then positioned in a six-degree-of-freedom robot and oriented and loaded in accordance with normative movement data in positions emulating upright posture and gait. Tekscan pressure sensors were positioned on the tibial plateau to record contact pressures in the tibio-femoral joint for different loading conditions. Results obtained from FE analyses and in-vitro tests on the same cadaveric knee were compared.

Results: Locations and values of compartmental forces and peak tibio-femoral contact stresses predicted from the FE model corroborated with those measured during the corresponding in-vitro tests on the cadaveric knee.

Discussion: This verified knee FE model can be used to evaluate the relative performances of different surgical techniques, improve clinical outcomes of surgical treatments, delay OA progression and the need for total knee replacements to reduce healthcare costs.

Introduction

Osteoarthritis (OA) is a debilitating degenerative disease involving all the tissues within the diarthrodial joint which often leads to significant pain, loss of joint function and is the leading cause of physical disability in the elderly. Radiographic studies of US and European populations show that 14.1% of men and 22.8% of women over 45 years of age show symptoms of knee OA (Valkenburg 1980). Age and obesity are both strong predictors of the development and progression of OA (Petersson, Jacobsson 2002). The World Health Organisation reports that OA accounts for 1% of total deaths in 2002 and is projected to be in the ten leading causes of disability adjusted life years (2.5%) in high-income countries in 2015 (Mathers, Loncar 2006). The reported total cost of OA on the UK economy is estimated at 1% of annual gross national product and $185.5 billion annually in the United States (Mathers, Loncar 2006). OA is problematic in the major load bearing joints (hip and knee) and can lead to significant loss of mobility and quality of life. There is no known cure for OA and current therapeutic approaches cannot arrest disease progression.

Joint malalignment (Sharma et al. 2010, Sharma et al. 2001), obesity (Messier 2009) and tissue injury (Potter et al. 2011, Stein et al. 2011, Lo et al. 2009) are primary biomechanical factors associated with osteoarthritis (OA) onset and progression. (Englund 2010). The aligned healthy knee is subjected to compressive loads of up to 2.5 times body weight during level walking. As little as 5° of varus mal-alignment ("bow-legged") increases the compressive loading in the medial compartment from 70% to 90% (Tetsworth, Paley 1994). Coventry explained how such a slight malalignment initiates a ‘vicious circle’, in which the resulting excessive stresses to localised cartilage, subchondral bone and the surrounding soft tissues produces more laxity and joint deformity, thereby repeating the cyclic degradation mechanism (Conventry 2001, Coventry 1965). This dramatic increase in compressive load corresponds to a fourfold

increase in the odds of medial tibio-femoral OA worsening over 18 months (Sharma et al. 2001).

Excessive joint stress is considered to be the common antagonistic load that damages the tissues within the diarthrodial joint irrespective of the specific biomechanical etiology. Therefore, it would be useful to know the knee joint contact stresses before and after surgical interventions to evaluate the relative effectiveness of the different treatment methods. This information would be useful to plan conservative surgical procedures to relieve damaged tissues from excessive loading, delaying the onset and progression of OA and the need for a total knee arthroplasty, which costs around £720 million in the UK alone. Although stress cannot be measured in vivo, it can be predicted from computational models.

Therefore, the **aim** of this study is to develop and verify a three-dimensional (3D) finite element (FE) model of a knee joint that integrates pre-operative imaging, motion analysis and computational biomechanics to predict post-operative tibio-femoral joint stress magnitude and location before and after simulated corrective surgery. Our ultimate goal is to use this validated FE model to predict the relative effectiveness of a number of surgical techniques for knee OA and other pathologies. Often, surgeons rely on a two-dimensional radiograph to crudely estimate the correction for a three-dimensional problem, which is influenced by dynamic loading. Understandably, these surgical outcomes have been unpredictable.

The **central hypothesis** is that our 3D FE knee model, which integrates subject-specific imaging and computational biomechanics, would predict post-operative knee joint mechanics. Specifically, we hypothesised that peak joint stress magnitude and location as well as compartment forces, predicted by our 3D subject-specific FE model during loading conditions emulating posture at the stance phase of gait, would corroborate the cadaveric in vitro results for different loading conditions.

Methods

A subject-specific FE model of a left cadaveric knee joint was created and verified by in vitro testing, emulating double stance posture and five quasi-static positions (heel strike, foot flat, peak knee adduction, heel off, and toe off) of the stance phase of gait. Results for 20° of flexion will be presented in this paper.

Imaging protocol of the knee

High-resolution medical resonance imaging (MRI) scans of a cadaveric knee were acquired, using an 8-channel transit-receive phased array knee coil. A 3D T1-weighted frequency fat-suppressed spoiled gradient recalled echo (SPGR) sequence and a 3D XETA scan sequence were used to generate a volumetric dataset for the segmentation of cartilage, bones, meniscus, and ligament structures for an accurate visualisation of each tissue (Figure 1). High resolution settings were used for the SPGR sequence (TE: 3ms, TR:14.6ms, acquisition-matrix: 512x512, NEX: 2, field-of view: 15cm, slice thickness: 0.6mm) and the 3D XETA (Gold et al. 2007) sequence (TE:33ms, TR: 2500ms, acquisition-matrix: 512x512, NEX: 0.5, field-of-view: 15cm, slice thickness: 0.6 mm). The in-plane resolution for both of the series was 0.29mm x 0.29mm.

Although computerised tomography (CT) images are commonly used to provide accurate geometry of bones, our previous study showed that discrepancy in geometry between CT and MRI images of different sequences was minimum (1.5% to 4.3%) at the joint line (centre of the field of view), where knee joint contact mechanics were computed (Mootanah et al. 2011). These accurate 3D MRI datasets were used to create FE models of each tissue.

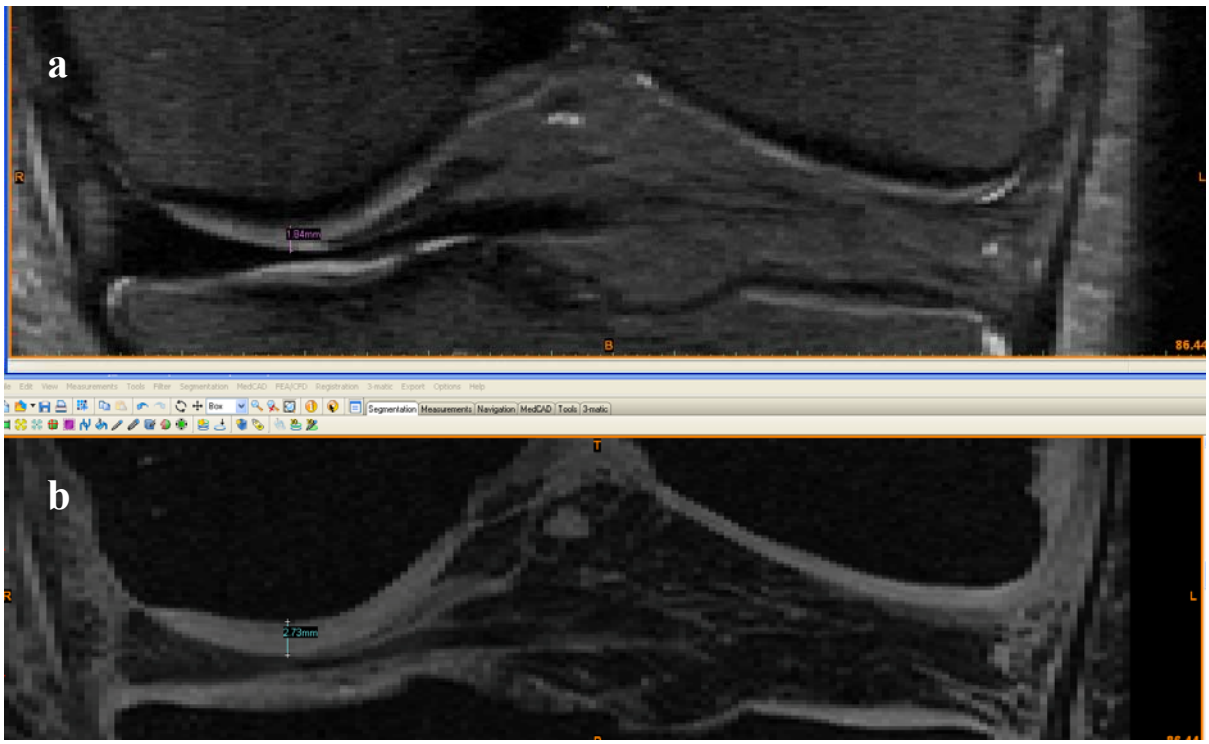

Figure 1: a. MRI images of the frontal view of the knee joint in (a) XETA sequence for accurate representation of meniscus and ligament and (b) SPGR sequence for accurate representation of cartilage and bone.

Accurate 3D models of the knee joint osseous and soft tissues

Dicom images of the SPGR and XETA MRI datasets of the cadaveric knee joint were imported into Mimics V14.2 (Materialise, Belgium). The XETA sequence was used to create accurate 3D representations of the medial and lateral menisci, the anterior and posterior cruciate ligaments and the medial and lateral collateral ligaments. The SPGR sequence was used to create accurate representations of the tibia, femur, fibula, as well as the medial and lateral tibial and femoral cartilages.

The 3D LiveWire tool was used as an interactive segmentation method to identify points lying at the tissue boundaries from the MRI images in all three planes (Figure 2). This segmentation method overcomes the challenges associated with imaging modalities (e.g. MRI) that do not support thresholding-based segmentation. The segmented boundaries of the different tissues were utilised to create 3D masks (Figure 2), which were then used to create accurate 3D models of the different tissues comprising the knee joint. The CAD and Primitive modules were used to create surfaces on the bones, for application of loading and boundary conditions when creating the FE model at a later stage. The quality of the surface mesh was improved, using the 3-matic re-meshing module of Mimics, to allow high quality 3D elements to be produced during the finite element meshing stage. The 3D knee joint assembly was then created so that material properties and boundary conditions could be applied to the different simulated tissues.

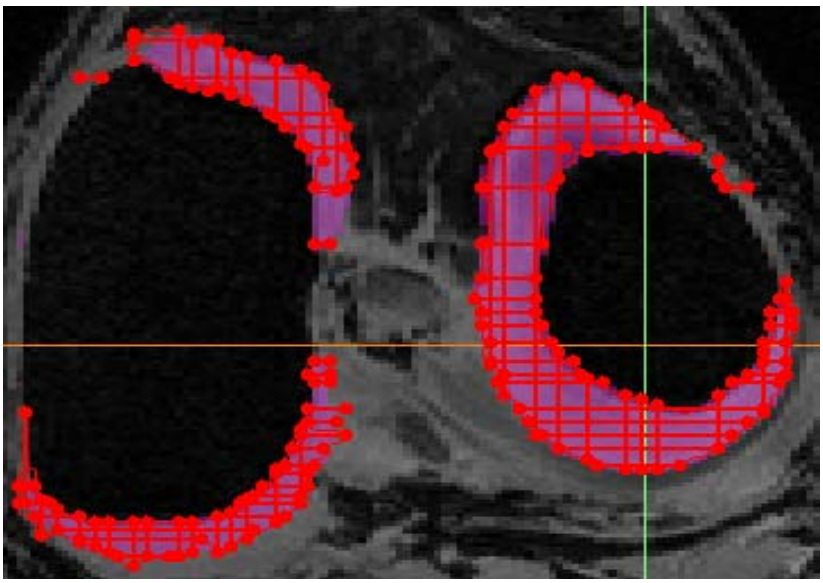

Figure 2: 3D LiveWire algorithm used to create accurate geometries of the different tissues.

Accurate 3D assembly of the knee joint

Common borders between adjacent masks were created to allow the application of boundary conditions. The ‘non-manifold’ tool in Mimics was employed for this purpose, to remove any gaps between the adjacent masks and to create a 'non-manifold assembly' of surfaces for the 3D osseous and soft tissue models. This method works very well for

structures with complex and irregular geometries such as the knee joint. When creating the 'non-manifold assembly', intersecting surfaces were deleted and boundary surfaces of objects that were in contact were generated (Figure 3). This procedure was repeated until all parts comprising the knee joint were included, one at a time.

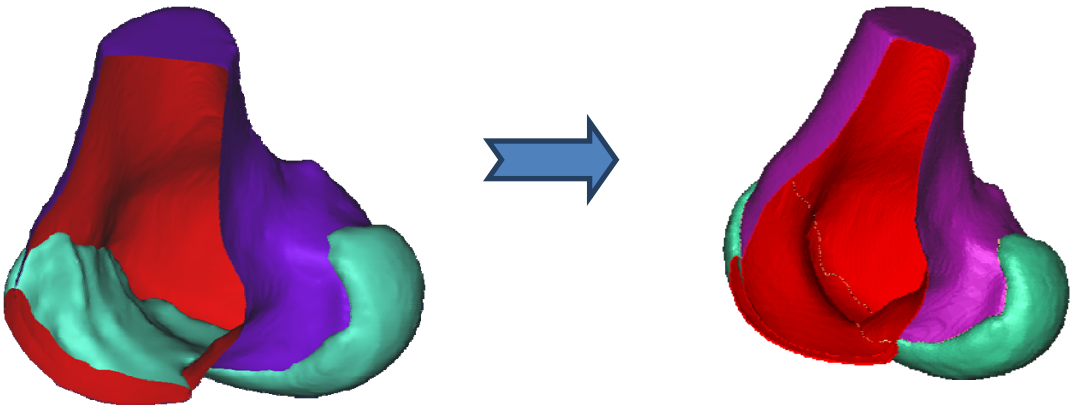

Figure 3. Non-manifold technique used to calculate a common border and remove gaps between adjacent surfaces

The knee joint surface assembly was exported to the computer aided design (CAD) package CATIA V5R18 (Dassault Systèmes, France), where accurate solid geometries of the osseous and soft tissues were created (Figure4) for the subsequent generation of a 3D FE knee model. In order to mesh the tissues with superior hexahedral elements, their edges were thickened in CATIA. This was accomplished by creating a 3D spline (Figure 5) around the edge of the structure, which was then employed to cut through the part to create a thick edge and enable the creation of hexahedral mesh.

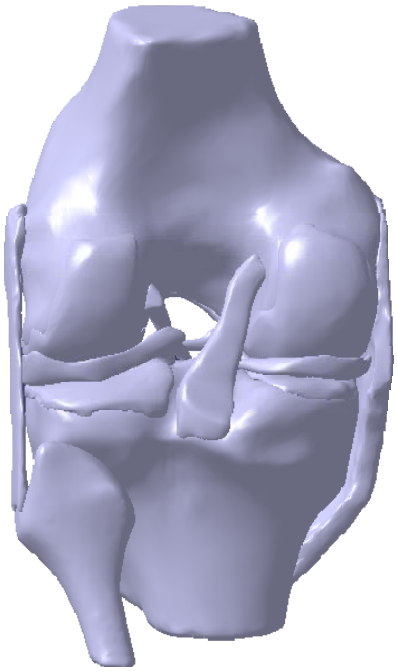

Figure 4. Solid geometry of the knee joint created in CATIA

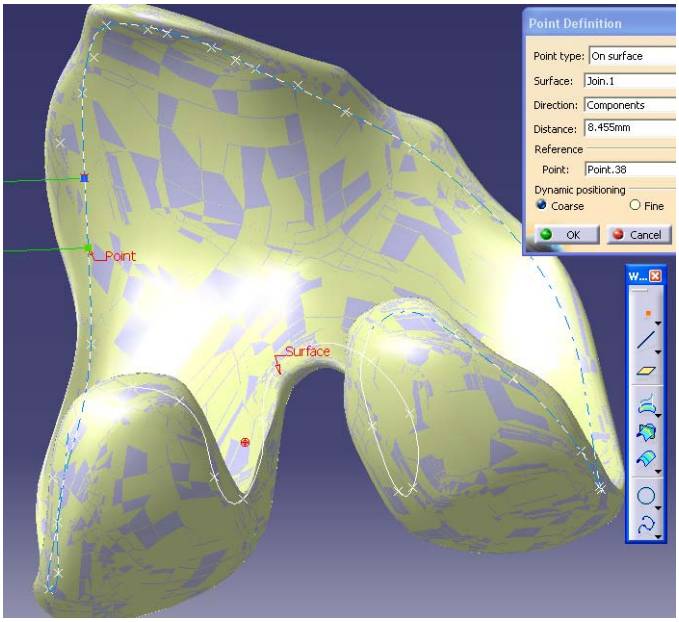

Figure 5: A 3D spline created on the surface of the FE cartilage is used to create a thickness along the edge for hexahedral meshing

Finite element model of the knee joint

Geometry

The geometrically accurate solid 3D knee joint assembly model (Figure 5) was exported to ABAQUS V6.11-2 (HKS, USA), and meshed in hexahedral elements (Figure 6).

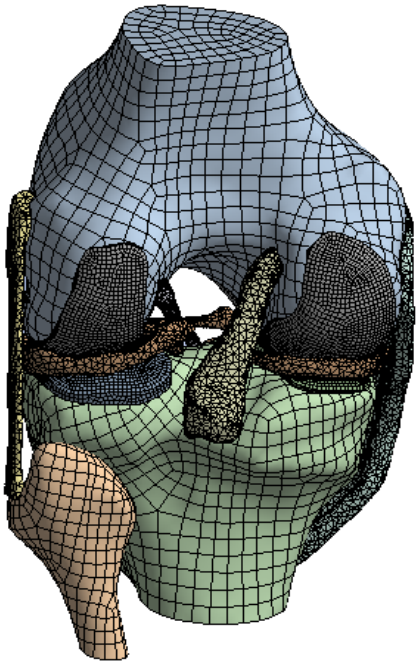

Figure 7: Finite element mesh of the knee

Material properties

Following sensitivity analyses, the material properties, shown in Table 1, were assigned to the knee osseous and soft tissues (Shepherd, Seedhom 1997, Shepherd, Seedhom 1999, Perie, Hobatho 1998, Schreppers, Sauren & Huson 1990, Weiss, Gardiner 2001).

Components	Young's Modulus (MPa)	Poisson's Ratio
Bone	1000	0.3
Cartilage	50	0.45
Meniscus	112	0.45
Ligament	400	0.45

Table 1: Material properties assigned to the different tissues comprising the knee joint

Boundary conditions

Attachment of each ligament and cartilage to the corresponding bone was modelled by merging the nodes on the corresponding surfaces that were previously created using the 3-matic routine. Cartilage-cartilage and cartilage-meniscus contact surfaces were simulated by creating contact elements between the corresponding surfaces (Figure 7). Each meniscal horn was attached to the tibial plateau by using the constraint definition capabilities in the FE packages.

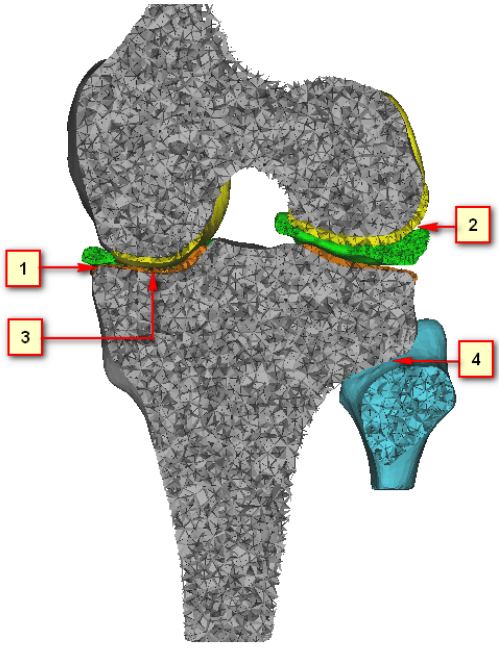

Figure 7. Boundary conditions, showing contact pairs between (1) tibial cartilage – meniscus, (2.) femoral cartilage – meniscus, (3.) femoral cartilage – tibial cartilage, (4.) tibia – fibula

Loading conditions

The loading conditions matched those of the in vitro tests on the cadaveric knee. The proximal femur was fixed in all six degrees of freedom (DOF), an axial load of 300N was applied to the distal tibia, simulating double stance position. A varus / valgus bending moment of 12Nm was then applied to the knee joint. A pretension was applied to the ligaments to eliminate any slack. Sensitivity analyses were carried out on element size and material properties of the different tissues to identify those parameters that the FE results are sensitive to.

In vitro investigations on cadaveric knee

The cadaveric knee was prepared for this validation study, using a Taylor Spatial Frame for accurate positioning of the knee joint (Figure 8a,b) (Rozbruch et al. 2010). Following stabilisation and calibration (Figure 8c), Tekscan pressure sensors were positioned on the tibial plateau (Figure 8d) and sutured to the base of the anterior cruciate ligament (Figure 8e) to record contact pressures in the tibio-femoral joint. The cadaveric knee was then positioned in a 6 DOF Kawasaki robot, with the proximal femur mechanically grounded to a floor mounted fixture and the tibia affixed to the robot gripper and 6DOF load cell (Figure 8f). The specimen was oriented in accordance with normative movement data (obtained from the Leon Root Motion Analysis Laboratory at HSS) in positions emulating upright posture and gait. This study focused on 20° flexion. An axial force of 300 N and a bending moment of 12 Nm varus and valgus were applied to the distal tibia. Medial and lateral compartment pressures and forces were measured with the TekScan IScan transducer in response to the externally applied forces and moments by the robot (Figure 8g). These experimental results were then compared with those predicted by the FE model of the knee joint for verification.

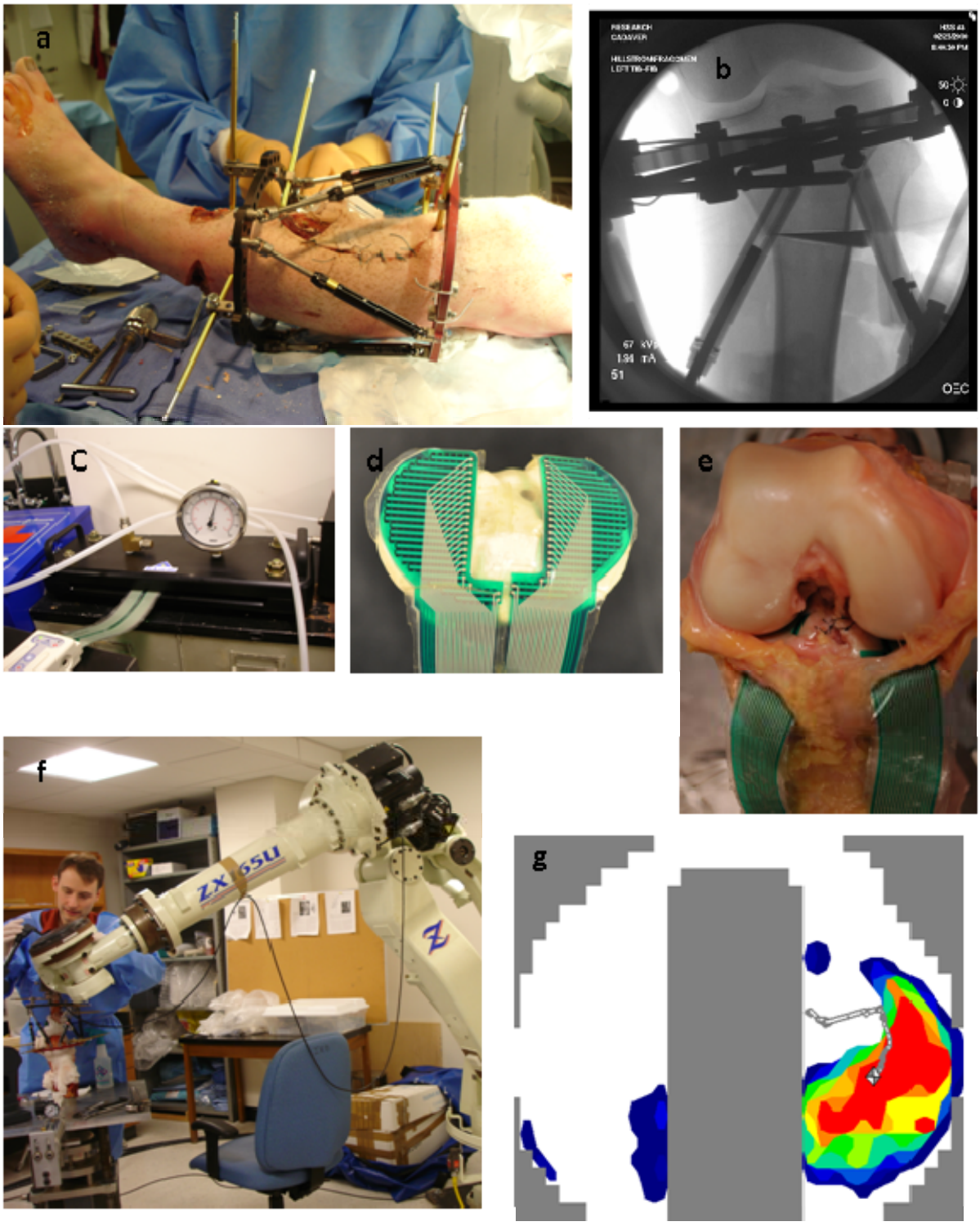

Figure 8: (a) Taylor Spatial Frame (TSF) fixed to cadaveric leg for model validation and future simulations of lower limb malalignments and corrections by high tibial osteotomy; (b) Fluoro of high tibial osteotomy with an applied corrective wedge geometry upheld by the TSF; (c) TekScan IScan calibration and stabilisation of (d) Tekscan sensors; (e) Tekscan sensors fixed to the cruciate ligaments between the tibial cartilage and the femur; (f) In-vitro testing on cadaveric knee, mounted on a 6 degrees-of-freedom Kawasaki robot for controlled loading; (g) pressure distribution and centre of pressure in joint following in vitro loading.

Results

Figure 9 illustrates the in vitro experimental and computational results for the loading conditions of a 300N axial force and a 12 Nm varus bending moment. The intra-articular pressure, as measured by the Tekscan transducer is shown in Figure 9a with a colour scale denoting the normal contact pressure in units of MPa. The normal stress (MPa) for the finite element model derived from the imaging data of the same cadaver specimen under identical loading conditions is shown in Figure 9b. The medial and lateral compartment forces (N) and peak pressure (MPa) from the experimental data is shown in Figures 9c and 9d versus time in seconds. The loading profile is 300N axial force at t = 0 seconds and 300N axial force plus 12Nm of bending moment at t = 21 seconds. Table 2 compares the values from the experimental data and computational model. The joint stress is within 7% and force within 25.6 % in the medial compartment.

Figure 10 illustrates the experimental and computational results for the loading conditions of a 300N axial force and a 12 Nm valgus bending moment. The intra-articular pressure measured in vitro is shown in Figure 10a and the corresponding normal stress (MPa), predicted by the FE model, is shown in Figure 11b. The medial and lateral compartment forces (N) and peak pressure (MPa) from the experimental data are shown in Figures 10c and 10d versus time in seconds. The loading profile is 300N axial force at t = 0 seconds and 300N axial force plus 12Nm of bending moment at t = 19 seconds. Table 3 compares the values from the experimental data and computational model. The joint stress is within 30.8% and force within 1.1 % in the lateral compartment.

12 Nm varus moment

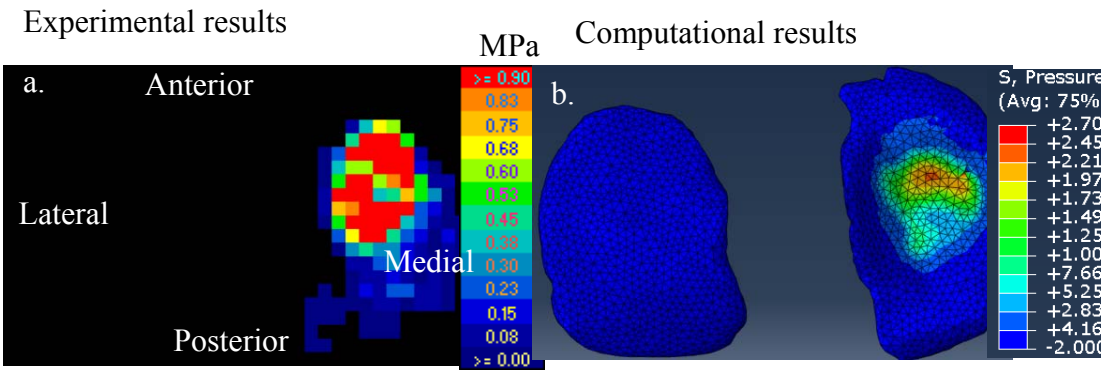

Forces in the medial and lateral compartment versus time during a ramp up to12Nm of varus moment followed by a ramp down

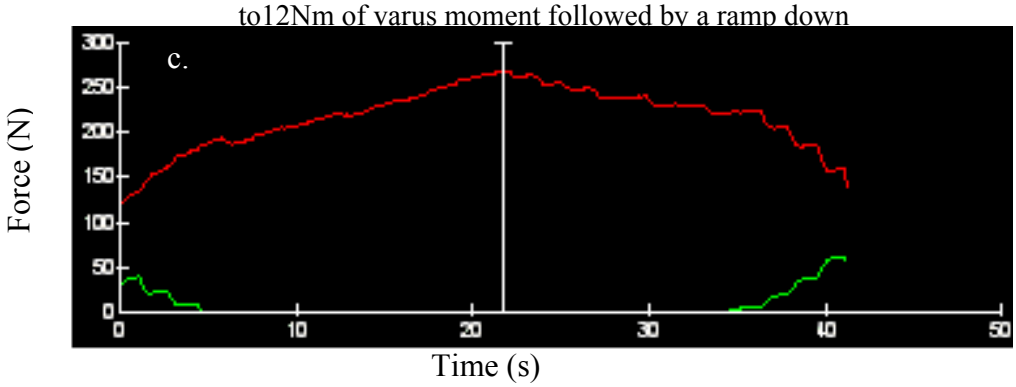

Peak pressures in the medial and lateral compartment versus time during a ramp up to12Nm of varus moment followed by a ramp down

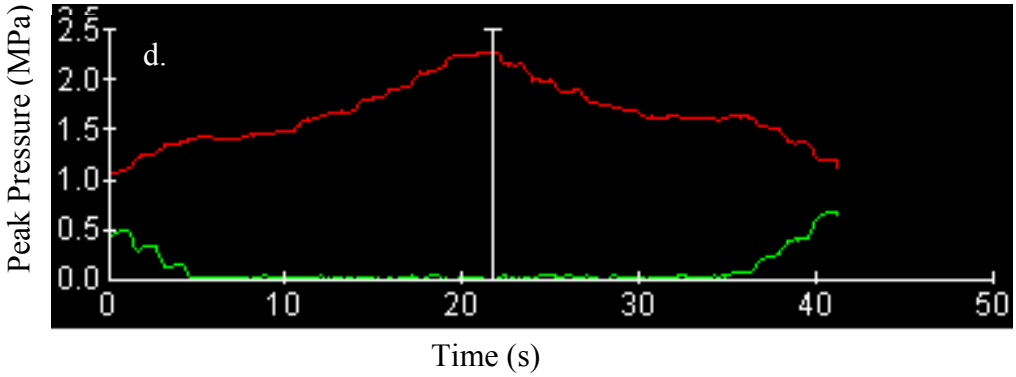

Figure 9: (a) in vitro contact pressure distribution; (b.) computer simulated pressure distribution in the medial and lateral tibial cartilage of a left knee after application of 300N axial force and 12Nm varus bending moment; (c.) graph of medial and lateral forces and (d) peak pressures after application of 300N axial force and 12Nm varus bending moment.

Table 2: Comparison of experimental and computational values of medial and lateral forces and peak pressures following application of 300N axial force and 12 Nm Varus moment

	σ_{lat} (MPa)	σ_{med} (MPa)	F_{lat} (N)	F_{med} (N)
Experimental	0.00	2.27	0	267.34
Computational	0.00	2.43	0	335.9
% Difference	0	7.0	0	25.6

12 Nm valgus moment

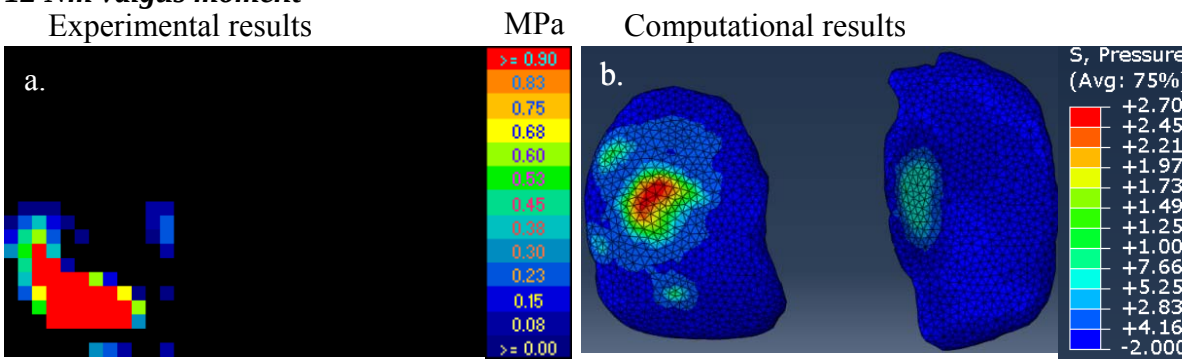

Forces in the medial and lateral compartment versus time during a ramp up to12Nm of valgus moment followed by a ramp down

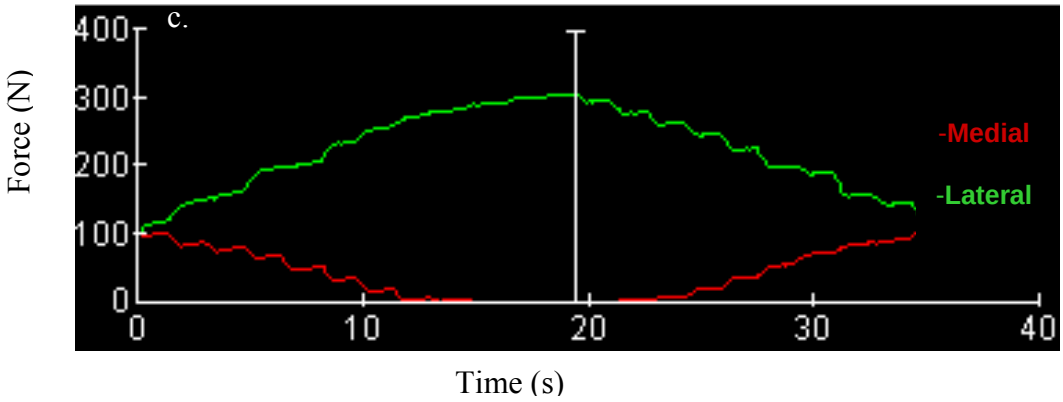

Peak pressures in the medial and lateral compartment versus time during a ramp up to12Nm of varus moment followed by a ramp down

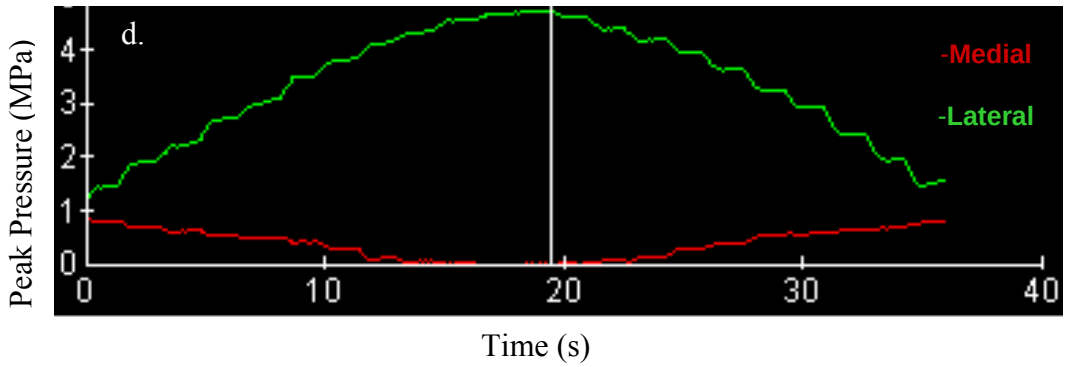

Figure 10: (a) in vitro contact pressure distribution; (b.) computer simulated pressure distribution in the medial and lateral tibial cartilage of a left knee after application of 300N axial force and 12Nm valgus bending moment; (c.) graph of medial and lateral forces and (d) peak pressures after application of 300N axial force and 12Nm valgus bending moment.

Table 3: Comparison of experimental and computational values of medial and lateral forces and peak pressures following application of 300N axial force and 12 Nm Valgus moment

	σ_{lat} (MPa)	σ_{med} (MPa)	F_{lat} (N)	F_{med} (N)
Experimental	4.74	0.00	305.06	0
Computational	3.38	0.8	308.66	85.35
% Difference	30.8	-	1.1	-

Discussion

A method for the development and validation of subject specific in-vitro knee stress models was presented. The subject specific finite element model of the knee employed tissue specific MRI scanning sequences and Mimics image processing software to represent the 3D shape and location of the bony and soft tissues comprising the diarthodial joint. The same in-vitro specimen from which the model was built was subjected to controlled loading in a robotic-based joint testing system. The FE model employed the same loading conditions. The joint forces and stresses from the FE model were in good agreement with those from in vitro studies, as shown in Figures 9-10 and Tables 2-3.

Although the results predicted by computer simulations corroborated those obtained experimentally, the subject specific FE knee model presented will be enhanced by addressing the following: the model requires evaluation at different knee angles spanning the full range of motion during functional activities (e.g. gait); the cartilage and meniscus will be represented by more realistic non-linear material properties and the ligaments will be represented by transversely isotropic hyperelastic materials (Gardiner, Weiss 2003); the patella, patellar and quadriceps tendons and musculo-tendinous forces will be included. Although the tissue geometries of the FE knee model were subject-specific, the material properties were acquired from the literature.

The ultimate aim of this investigational team is to use this approach for subject-specific surgical planning of HTO to improve surgical outcomes. Future efforts will address current model limitations and consider loading conditions and joint angles that emulate

the stance phase of gait and other activities of daily living. In addition, the model will be applied to in-vivo test subjects towards achieving our ultimate aim.

Each year in the USA, 5,000,000 patients will report to their doctors with significant knee pain but only 500,000 will require surgery (Buckholtz, 2011). There are currently no standard of care protocols for the conservative management of knee OA for the remaining 4.5 million patients. The current treatments available are physical therapy, nutraceuticals (glucosamine, chondroitin sulfate), viscosupplementation (high molecular weight hyaluronic acid), weight loss, orthoses (knee braces and foot orthoses), assistive devices, Platelet Rich Plasma or any combination of the afore-mentioned therapies. The evidence for each of these modalities is in many cases controversial and the evidence for combinational therapies is almost nonexistent. Given that the HTO actually does not violate the joint, it may be considered a conservative procedure for treating the patient with knee OA. If perfected, such a model may become the subject specific tool required to guide orthopaedic surgeons to achieving the realignment of the genuvarum or genuvalgum knee that minimises excessive stress to the tissues within the joint.

Recent projections of total knee and hip replacement procedures in the US and UK will approach 1% of the gross national product by 2030, which is clearly an unsustainable trajectory. Joint sparing procedures that may be tuned to the individual patient's morphometric requirements are needed. Innovative approaches to developing validated subject specific models based upon the 3D imaging data of the patient are anticipated to play a critical role for the preservation of the diarthrodial joint with OA, reducing patient's pain while improving their function, and addressing the predicted escalation in total joint replacements. This project represents the first step towards this important

application, which is to validate the capability of a subject specific model for predicting joint forces and stresses experienced under load.

References

Conventry, M.B. 2001, "Osteotomy of the upper portion of the tibia for degenerative arthritis of the knee. A preliminary report by Mark B. Conventry, MD. From the Section of Orthopedic Surgery, Mayo Clinic and Mayo Foundation, Rochester, Minnesota. 1965", *The Journal of bone and joint surgery.American volume,* vol. 83-A, no. 9, pp. 1426.

Coventry, M.B. 1965, "Osteotomy of the Upper Portion of the Tibia for Degenerative Arthritis of the Knee. a Preliminary Report", *The Journal of bone and joint surgery.American volume,* vol. 47, pp. 984-990.

Englund, M. 2010, "The role of biomechanics in the initiation and progression of OA of the knee", *Best practice & research.Clinical rheumatology,* vol. 24, no. 1, pp. 39-46.

Gardiner, J.C. & Weiss, J.A. 2003, "Subject-specific finite element analysis of the human medial collateral ligament during valgus knee loading", *Journal of orthopaedic research : official publication of the Orthopaedic Research Society,* vol. 21, no. 6, pp. 1098-1106.

Gold, G.E., Busse, R.F., Beehler, C., Han, E., Brau, A.C., Beatty, P.J. & Beaulieu, C.F. 2007, "Isotropic MRI of the knee with 3D fast spin-echo extended echo-train acquisition (XETA): initial experience", *AJR.American journal of roentgenology,* vol. 188, no. 5, pp. 1287-1293.

Lo, G.H., Hunter, D.J., Nevitt, M., Lynch, J., McAlindon, T.E. & OAI Investigators Group 2009, "Strong association of MRI meniscal derangement and bone marrow lesions in knee osteoarthritis: data from the osteoarthritis initiative", *Osteoarthritis and cartilage / OARS, Osteoarthritis Research Society,* vol. 17, no. 6, pp. 743-747.

Mathers, C.D. & Loncar, D. 2006, "Projections of global mortality and burden of disease from 2002 to 2030", *PLoS medicine,* vol. 3, no. 11, pp. e442.

Messier, S.P. 2009, "Obesity and osteoarthritis: disease genesis and nonpharmacologic weight management", *The Medical clinics of North America,* vol. 93, no. 1, pp. 145-59, xi-xii.

Mootanah, R., Imhauser, C., Koff, M.F., Potter, H.G. & Hillstrom, H.J. 2011, "MRI Sequence Influences Geometrical Interpretation of Osseous Tissues", *Orthopaedic Research Society*.

Perie, D. & Hobatho, M.C. 1998, "In vivo determination of contact areas and pressure of the femorotibial joint using non-linear finite element analysis", *Clinical biomechanics (Bristol, Avon),* vol. 13, no. 6, pp. 394-402.

Petersson, I.F. & Jacobsson, L.T. 2002, "Osteoarthritis of the peripheral joints", *Best practice & research.Clinical rheumatology,* vol. 16, no. 5, pp. 741-760.

Potter, H.G., Jain, S.K., Ma, Y., Black, B.R., Fung, S. & Lyman, S. 2011, "Cartilage Injury After Acute, Isolated Anterior Cruciate Ligament Tear: Immediate and Longitudinal Effect With Clinical/MRI Follow-up", *The American Journal of Sports Medicine, .*

Rozbruch, S.R., Segal, K., Ilizarov, S., Fragomen, A.T. & Ilizarov, G. 2010, "Does the Taylor Spatial Frame accurately correct tibial deformities?", *Clinical orthopaedics and related research,* vol. 468, no. 5, pp. 1352-1361.

Schreppers, G.J., Sauren, A.A. & Huson, A. 1990, "A numerical model of the load transmission in the tibio-femoral contact area", *Proceedings of the Institution of Mechanical Engineers.Part H, Journal of engineering in medicine,* vol. 204, no. 1, pp. 53-59.

Sharma, L., Song, J., Dunlop, D., Felson, D., Lewis, C.E., Segal, N., Torner, J., Cooke, T.D., Hietpas, J., Lynch, J. & Nevitt, M. 2010, "Varus and valgus alignment and incident and progressive knee osteoarthritis", *Annals of the Rheumatic Diseases,* vol. 69, no. 11, pp. 1940-1945.

Sharma, L., Song, J., Felson, D.T., Cahue, S., Shamiyeh, E. & Dunlop, D.D. 2001, "The role of knee alignment in disease progression and functional decline in knee osteoarthritis", *JAMA : the journal of the American Medical Association,* vol. 286, no. 2, pp. 188-195.

Shepherd, D.E. & Seedhom, B.B. 1999, "Thickness of human articular cartilage in joints of the lower limb", *Annals of the Rheumatic Diseases,* vol. 58, no. 1, pp. 27-34.

Shepherd, D.E. & Seedhom, B.B. 1997, "A technique for measuring the compressive modulus of articular cartilage under physiological loading rates with preliminary results", *Proceedings of the Institution of Mechanical Engineers.Part H, Journal of engineering in medicine,* vol. 211, no. 2, pp. 155-165.

Stein, V., Li, L., Lo, G., Guermazi, A., Zhang, Y., Kent Kwoh, C., Eaton, C.B. & Hunter, D.J. 2011, "Pattern of joint damage in persons with knee osteoarthritis and concomitant ACL tears", *Rheumatology international, .*

Tetsworth, K. & Paley, D. 1994, "Malalignment and degenerative arthropathy", *The Orthopedic clinics of North America,* vol. 25, no. 3, pp. 367-377.

Valkenburg, H. 1980, "Clinical versus radiological osteoarthritis in the general population." in *Epidemiology of Osteoarthritis*, ed. J. Peyron, Ciba-Geigy, Paris, pp. 53-58.

Weiss, J.A. & Gardiner, J.C. 2001, "Computational modeling of ligament mechanics", *Critical Reviews in Biomedical Engineering,* vol. 29, no. 3, pp. 303-371.